Eurographics Symposium on Rendering (2022)
A. Ghosh and L.-Y. Wei (Guest Editors)

Spectral Upsampling Approaches for RGB Illumination

G. C. Guarnera[1,2,3], Y. Gitlina[4], V. Deschaintre[4,5] and A. Ghosh[1,4]

[1]Lumirithmic Ltd
[2]University of York, United Kingdom
[3]Norwegian University of Science and Technology, Norway
[4]Imperial College London, United Kingdom
[5]Adobe Research, United Kingdom

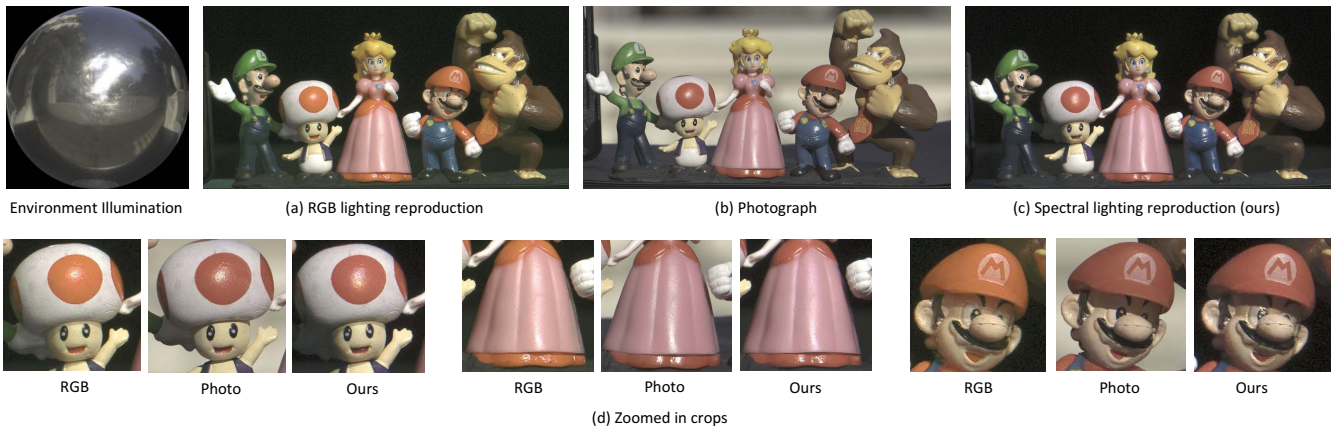

Figure 1: *Comparison of toy figurines photographed in an outdoor lighting environment (b), and corresponding lighting reproduction inside a multispectral LED sphere using RGB LEDs (a), vs spectral lighting reproduction inside the LED sphere using our proposed spectral upsampling method (c). As can be seen, our RGB-to-spectral upsampling of the input RGB lightprobe achieves a closer qualitative lighting reproduction on the figurines compared to simply driving the LED sphere with RGB values.*

Abstract

We present two practical approaches for high fidelity spectral upsampling of previously recorded RGB illumination in the form of an image-based representation such as an RGB light probe. Unlike previous approaches that require multiple measurements with a spectrometer or a reference color chart under a target illumination environment, our method requires no additional information for the spectral upsampling step. Instead, we construct a data-driven basis of spectral distributions for incident illumination from a set of six RGBW LEDs (three narrowband and three broadband) that we employ to represent a given RGB color using a convex combination of the six basis spectra. We propose two different approaches for estimating the weights of the convex combination using – (a) genetic algorithm, and (b) neural networks. We additionally propose a theoretical basis consisting of a set of narrow and broad Gaussians as a generalization of the approach, and also evaluate an alternate LED basis for spectral upsampling. We achieve good qualitative matches of the predicted illumination spectrum using our spectral upsampling approach to ground truth illumination spectrum while achieving near perfect matching of the RGB color of the given illumination in the vast majority of cases. We demonstrate that the spectrally upsampled RGB illumination can be employed for various applications including improved lighting reproduction as well as more accurate spectral rendering.

CCS Concepts

• ***Computing methodologies*** → ***Rendering; Image and video acquisition;***

1. Introduction

Illumination is one of the fundamental elements of virtual scenes alongside shape/geometry and materials and has a major effect on the overall scene appearance. Modern rendering software allows to render scenes with complex spectral reflectance and illumina-

tion ([NDVZJ19, PJH16]), allowing to precisely simulate optical phenomenon such as iridescence, refraction or diffraction. Spectral illumination has also been demonstrated to improve the accuracy of on-set lighting reproduction [WHD03, LYL*16]. However, the main challenge for any of these applications is that spectral data for illumination is not commonly available.

While recent works have proposed to facilitate RGB to spectral *reflectance* upsampling for driving spectral rendering [JH19, MY19], the creation or acquisition of spectral *illumination* remains a challenge, particularly for environmental illumination. Previous work on spectral upsampling has relied on the smoothness of reflectance spectra, a property not shared by most illumination spectra. In this work, we present practical approaches for high fidelity spectral upsampling of RGB illumination, including image-based representations such as light probes, and demonstrate its application in improved spectral lighting reproduction and more accurate spectral rendering.

Given an illuminant RGB color, our approach combines 6 basis spectra to create a metamer illuminant spectrum. We demonstrate our results by upsampling legacy RGB HDR environment maps to a spectral representation. In addition to the spectral rendering possibilities enabled by this solution, it also enables more accurate lighting reproduction using a multispectral LED sphere (see Fig. 1).

Our proposed solution relies on a basis composed of 6 RGBW LEDs mixing narrowband and broadband spectra. We propose two different approaches for estimating weights of this basis given input RGB color: using (a) Genetic algorithm based optimization, and (b) using neural networks. Additionally, we discuss other bases with our approach including a theoretical Gaussian basis, and an alternate LED bases previously employed for multispectral lighting [LYD17].

We carefully validate our method against measured spectra and demonstrate good qualitative results on both object relighting and color checker reflectance reconstruction. We demonstrate our results to be of comparable quality to the state-of-the-art method of LeGendre et al. [LYL*16] *without* requiring additional reference color chart measurements. We also compare our approach to reflectance spectral upsampling methods [JH19, MY19] and confirm that our approach allows to better reconstruct non smooth illumination spectra.

To summarize, in this paper we propose the following contributions:

- Practical RGB to spectral upsampling approaches for illumination with a compact basis representation.
- A Genetic algorithm for basis optimization and a cascaded feed-forward neural network for basis-driven spectral upsampling.
- Evaluation of multiple bases for spectral lighting representation.

2. Previous Work

In the following, we discuss the background and the most relevant related work.

Background: The human eye contains three types of cone cells, each with a different sensitivity to a broad range of light wavelengths. Each cone i integrates spectral data over the visible range $\omega = [380nm - 780nm]$: overall, cones act as color receptors and allow trichromatic vision:

$$c_i = \int_\omega f_i(\lambda) s(\lambda) d\lambda \tag{1}$$

where $c = [c_1, c_2, c_3]$ is the color response, $f_i(\lambda)$ is the spectral sensitivity of cones of type i, $s(\lambda)$ is a spectrum, either an illuminant spectral power distribution or the light reflected by a surface with a given spectral surface reflectance; $\lambda \in \omega$ is the wavelength. CIE has defined a standard observer, with published spectral responses (*Color Matching Functions* $\bar{x}(\lambda)$, $\bar{y}(\lambda)$ and $\hat{z}(\lambda)$), leading to the CIE XYZ tristimulus color space [WS82]. The integration performed by the cone cells compresses the complete spectral information into just three sensory quantities, thus leading to a phenomenon known as *metamerism*, that arises when two different spectra s_1 and s_2 defined *metamers* [CIE86], generate the same tristimulus values:

$$\int_\omega f_i(\lambda) s_1(\lambda) d\lambda = \int_\omega f_i(\lambda) s_2(\lambda) d\lambda, i = 1,2,3. \tag{2}$$

The concept of metamerism is not limited to human observers, but can be extended to any imaging system with three spectral channels [FRJ01]; similar considerations apply to monochrome sensors. In general, the recovery of the original spectral information from trichromatic colors is severely underconstrained. In theory, each color can be generated by an infinite number of different spectra [Har01, MY19, PMHD19]. However, the frequency of metamerism in outdoor natural scenes, where the illumination is given by daylight at different color-correlated temperatures, is relatively rare [FF12, ABS16, AG18]; in the reflective case, there are significantly less metameric matches for complex or saturated reflective spectra than for simpler and neutral ones.

Lighting Reproduction: RGB light probes [Deb98] record the incident illumination at a specific location, typically by stitching together fisheye images from different directions or by acquiring a HDR sequence of a mirrored sphere. As demonstrated by Debevec et al. [DGBB12], the inclusion of diffuse strips between the quadrants of a cut-apart mirrored sphere allows the estimation of the full dynamic range from a single photograph. Such light probes can then be used for rendering virtual objects [Deb98] or for lighting reproduction applications, for instance by driving colour and intensity of inward pointing LED lights in spherical domes [DHT*00, UWH*03, LYL*16]. However, relying solely on RGB LEDs for real-world lighting reproductions leads to poor color rendition and visible color casts, particularly when directly minimizing the sum of the square residuals of the reproduction light spectra to the target illuminant (Spectral Illumination Matching - SIM) [WHD03], due to gaps in the spectral power distribution of the resulting illumination. By increasing the number of LEDs beyond RGB, it is possible to significantly improve the quality of lighting reproduction results, matching a wider set of real-wold illuminants. Similarly, relighting applications can benefit from more accurate spectral reflectance estimation achievable with a 5-LED basis [PLGN07]. Legendre et al. [LYD17] demonstrated that by accounting for the color rendition capabilities of different LED basis in a lighting reproduction setup, material color appearance under arbitrary lighting can be accurately matched with just 5 LEDs. Legendre et al. [LYL*16] proposed a Metameric Reflectance Matching (MRM) technique, which requires a specialized physical setup con-

sisting of 5 oriented color charts that have to be measured along with a light probe in order to drive a multispectral LED sphere with 6 types of LEDs. Unlike the approach of Legendre et al., our proposed method focuses on Metameric Illuminant Matching (MIM) and does not require any other information besides RGB illumination as input (such as a light probe) for the spectral upsampling step. In this respect, our method can be used for spectral conversion of any recorded legacy RGB illumination, for which a color chart is often not included, and it allows driving a multispectral lighting system with just RGB input. Overall, our method is more general and applies to non-LED bases and has broader applications in spectral rendering and AR. While [LYL*16] does not require the use of specialized equipment for camera characterization, the use of color charts is common in illuminant estimation techniques [GRB*08, HFG*20].

Illumination Estimation: Estimating the scene illuminant from RGB image data, either as a spectrum or a RGB color [BCS17], is the main step in computational color constancy [Ebn07], with a number of applications, ranging from color imaging to computer vision. Often, the key assumption is that there is only a single, dominant illuminant in the scene [GRB*08]. While 3 variables are necessary and sufficient to define a color [Gra53], due to metamerism more than three channels are required to obtain a device-independent estimate of an illuminant spectrum [Har01]. Ratnasingam and Hernández-Andrés [RHA11] focused on daylight illumination to demonstrate accurate per-pixel recovery of spectral data from 6 channels input data, modelling the Camera Spectral Sensitivities (CSSs) as Gaussian functions and constructing an illuminant invariant feature space from a large set of measured reflectances. Tominaga and Tanaka [TT06] demonstrated spectral estimation from spherical RGB images, for mixed daylight and incandescent bulb illumination, under the assumption that the CSSs are known, and that spectra in the input image can be expressed as a linear combination of three basis spectra; the basis are obtained as the first three principal components of a dataset containing both CIE standard illuminants and measured light sources [Tom96]. In order to deal with spiky fluorescent spectra, Tominaga and Tanaka [TF07] extended the number of basis to 5 and replaced the RGB camera with a monochrome camera equipped either with 6 gelatin filters or a liquid-crystal tunable filter, used to sample the visible spectrum using up to 61 narrow bands; for each spectral band, the corresponding CSS must be known. As opposed to these work, we do not perform SIM and do not attempt to recover the unknown illuminant spectrum from the incomplete RGB information. Instead, our work focuses on per-pixel MIM, providing a plausible spectrum that visually matches the reference color for a human observer.

Spectral Upsampling: In general, most techniques for spectral estimation greatly benefit from accurate camera characterization, required to convert device-dependent RGB data to device-independent CIE XYZ tristimulus values [KK08, GBS19]. Shi et al. [SYH*14] estimate the incident illumination spectrum from the photograph of a color chart with known spectral reflectances, used to compute the corresponding CIE XYZ values. Similar concepts have been applied to spectral reflectance estimation from RGB data (*spectral upsampling*), with some key differences, since spectral reflectance is the ratio of the reflected light to the incident light and thus defined in the range $[0-1]$, while emission spectra are unbounded. Furthermore, reflectance spectra are typically very smooth in the visible range [Wan87], while emission spectra can display sharp peaks and have complex shapes, such as in the case of fluorescent lamps. A third important point is that some CIE XYZ triplets (therefore, some chromaticities), cannot be obtained from reflectance spectra, thus leading to concept of gamut of solid reflectances. Bianco [Bia10] proposed a method based on local optimization, aimed at recovering smooth, metameric reflectance spectra from user-specified tristimulus values. Meng et al. [MSHD15] precompute spectra for a set of points forming a regular grid on the 2D CIE 1931 *xy* chromaticity diagram. To compute the spectrum corresponding to arbitrary CIE XYZ values, the precomputed spectra are interpolated, either using bilinear or barycentric interpolation, depending on their location on the chromaticity diagram. Since the resulting spectrum might not conserve energy, a normalization step is required, potentially introducing errors [JH19]. Jakob and Hanika [JH19] focused on the sRGB color space, defining a 3 dimensional non-linear function space, whose coefficients are precomputed and stored in a 3D table that account also for the brightness; the coefficients are then converted into a spectrum at runtime. The advantage of explicitly accounting for brightness is the ability to produce smooth spectra even in case of dark input colors. Jung et al. [JWH*19] addressed material beyond the gamut of solid reflectances, including a fluorescent component expressed in parametric form. Using optimization, Mallett and Yuksel [MY19] defined three spectral primaries that allow to obtain relatively smooth, energy conserving reflectance spectra as a linear combination of the primaries, for any given input sRGB triplet. Peters et al. [PMHD19] introduced a compact representation for reflectance spectra with known shape, complemented by a lookup table approach for assets stored in three color channels. They demonstrated that with three to six scalars per pixel (4 to 8 bytes per pixel), any reflectance spectra can be accurately reconstructed by their bounded maximum entropy spectral estimate. In case of emission spectra, the number of coefficients m required for a satisfactory reconstruction can be significantly higher (16 to 32), as well as the run time of their algorithm, with complexity $\mathcal{O}(m^2)$. While their approach has the ability to encode very complex illumination spectra, it requires a known spectrum for computing the coefficients. Instead, our employed basis focuses on compactly representing many common illumination spectra while requiring only the corresponding RGB color as input. Similarly to [JH19], Tódová et al. [TWF21] proposed the use of a pre-computed sRGB coefficient cube to map colors to the corresponding moment based representation of the reflectance spectra [PMHD19]. Their method allows to input a set of constraints, i.e. user-supplied spectra for some sRGB colors, that are closely preserved by the moment based representation and used as priors for the optimization of neighbouring colors in the cube. Fubara et al. [FSD20] proposed CNN-based upsampling of RGB images, using a modified UNet to jointly learn a set of 10 basis functions and the weights. Given the lack of indoor hyperspectral images, particularly under complex illuminants, their method is limited to natural outdoor illumination.

3. Method

We propose two different procedures for converting measured RGB values of different illuminants into the spectral domain us-

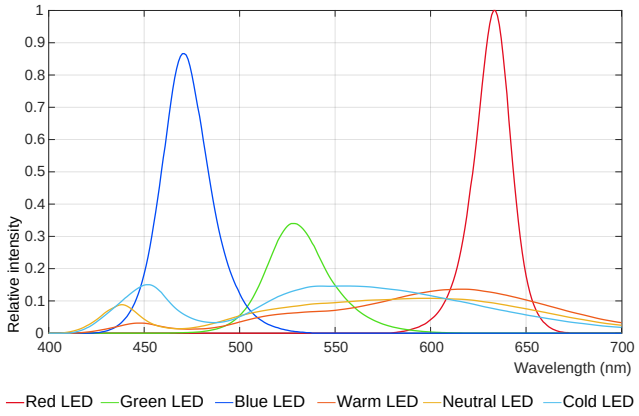

Figure 2: *Spectral power distributions of 6 different LED types employed as the basis for spectral upsampling of RGB illumination.*

ing a linear combination of selected illumination basis spectra. This includes a Genetic algorithm based optimization described in Sec. 3.2, and a neural upsampling procedure described in Sec. 3.3. Our method assumes the input RGB color has been acquired using a camera with reasonable color processing (e.g., sRGB colorspace with daylight white balance setting). We first describe our choice of basis for the spectral upsampling procedures in Sec. 3.1, which is primarily motivated by practical spectral lighting reproduction.

3.1. Spectral basis selection

We choose a relatively compact basis of 6 illuminant spectra as we want to minimize the storage overhead compared to RGB. The size of basis is also motivated by the previous work of Legendre et al. [LYL*16] who show that a set of 6 LEDs allows to cover most of the illumination spectrum.

We define our basis using the set of measured spectral power distributions (SPDs) of the 6 LED types installed in a multi-spectral LED sphere that we have access to. Namely, three narrowband Red, Green, and Blue LEDs, and three broadband white LEDs (warm 2700K, neutral 4000K, and cool 5700K). We measure the SPDs of these LEDs with a spectrometer –Sekonic SpectroMaster C700– by placing it at the center of the LED sphere. Our measured spectral basis is shown in Figure 2.

Unless stated otherwise, our results are shown with the above described basis. We however highlight that our method is not limited to a specific basis and demonstrate it with the LED basis set employed by Legendre et al. and an alternate theoretical basis using a set of Gaussians later in Section 4.5 (see Fig. 10).

To drive the multispectral light stage and to compute its dynamic range and the white point, as required by the color space conversions embedded both in our initialization and optimization, we recover the absolute value of each LED SPD, expressed in $w/(m^2 \cdot sr \cdot nm)$. The CIE XYZ white point of the device used in this work, measured with all LEDs on at full intensity, is $[909, 897, 784] cd/m^2$. Such measurements are required only once, and can be obtained with a spectroradiometer or using a colorimetrically characterized camera, with support for the absolute scale [GBS19]. Please note that just the knowledge of the relative intensity of the LED SPDs, as shown in Fig. 2, would suffice for most practical applications.

3.2. Genetic algorithm based optimization

To reconstruct the target illuminant color and spectrum, we propose an optimization procedure to find a set of weights α_k^* to linearly combine a given set of n basis spectra. To guide this optimization, we minimize the ΔE_{94} color difference [CIE95] between the CIELab values of the reference illumination and our reconstructed spectrum:

$$\arg\min_{\alpha_k^*} \left\{ \Delta E_{94}(Lab_{ref}, XYZ \rightarrow Lab[\sum_{k=1}^{n} \sum_{\lambda=400}^{700} \alpha_k S_{k,\lambda}^* x\bar{y}x(\lambda)]) \right\}, \tag{3}$$

where Lab_{ref} is the Lab color of the target illuminant, $XYZ \rightarrow Lab$ represents a standard conversion that maps CIE XYZ values to the Lab color space, S_k^* is a set of basis spectra and $x\bar{y}z(\lambda)$ are the CIE 1931 2° Color Matching Functions (CMFs). While our method is not limited to a specific colorspace (e.g. it works with sRGB, Adobe RGB, Rec. 2020 etc.), the colorspace in use must be known, in order to convert the illuminant color to the corresponding CIE XYZ value and then to CIE Lab.

Given the one-to-many relationship between trichromatic colors and possible metamers (see Sec. 2), we found convex optimization techniques likely to get stuck in local minima. Therefore, to compute the set of weights α_k^* we use a stochastic search strategy based on genetic algorithms (GA). A comparison between our approach and interior point convex non-linear optimization is reported in the supplemental material, as well some examples showing the non-convexity of the optimization problem addressed by our work.

In our implementation, the set of individuals that will contribute to the definition of the next generation are selected by means of pair-wise comparisons in a tournament selection, where pairs are randomly picked. From this set, parents are selected according to panmixia; the crossover of their DNA (i.e. their coordinates) is given by the arithmetic mean. While this solution allows to reduce the algorithm complexity, it tends to destroy recessive genes in a small number of generations [Dav51]. To mitigate this effect, 10% of the individuals for a subsequent generation are produced by applying small mutations to the coordinates of a single parent (power mutation [DSKM09]), while the 10% best performing individuals are included in the next generation. We discretize the parameter domain over a regular 6D lattice, constraining each variable to be an integer in the range $[0-255]$, thus directly corresponding to the activation value of an LEDs in the LED sphere; the rules to create the initial population and the following ones are modified in order to enforce such constraints [DSKM09]. Using the weight range restriction for each element of the basis in the linear combination, we ensure that the physical LEDs will be capable of reproducing the intensity of the target spectra.

While GAs do not require to specify an initial parameter guess, in our implementation we include the possibility to initialize the population relying on barycentric interpolation, for which the contribution of each basis spectrum corresponds to the inverse of its

distance to the target illuminant color in the CIE Lab color space. Each starting weight of one individual are computed as follows:

$$W_k = \frac{1}{N} * \frac{1}{\Delta E_{94}(Lab_{ref}, Lab_k)}, \tag{4}$$

where N is a normalization factor computed as $\sum_{k=1}^{n} \frac{1}{Wk}$, Lab_{ref} is the Lab color of the target illuminant and Lab_k is the CIE Lab color of k^{th} basis spectrum.

The other individuals of the initial population (overall 60 individuals) are located in the neighborhood of Eq. 4, with weights randomly chosen according to a uniform distribution in the interval $W_k \pm 5\%$, if within the $[0-255]$ range. In our experiments, the GA performance is mostly affected by the size of initial population, with smaller values than the one used in this work leading to suboptimal solutions, while a larger population size does not appear to improve the results. While we set an upper bound to the number of generations (600), the number of iterations required is typically reduced by keeping track of the relative change in the fitness of the best performing individuals in the previous 50 generations, stopping if this falls below a predefined threshold. Our method's average run-time (single thread unoptimized implementation) is 5.09s/color on a AMD Ryzen 7 2700 3.20 GHz processor and 32GB RAM desktop PC.

3.3. Neural upsampling

The optmization-based approach might become unpractical when a large number of colours need to be upsampled. Therefore, we propose learning the mapping $f : \mathcal{R}^3 \rightarrow \mathcal{R}^n$ from tristimulus colors to their n spectra basis metameric representation. We optimize the weights and biases of a fully-connected multilayer perceptron (MLP), in which each layer following the first hidden one has connections coming not only from the previous layer, but also from the input and all previous layers (Cascade-Forward Neural Network - CFNN); Fig. 3 reports a schematic representation of a CFNN with 2 hidden layers. In addition to modelling the non-linear relationship between input and output, direct connections between layers allow to better preserve linear relationships between them [WSSY18].

These characteristics allows to enforce properties such as: $f([X_a, Y_a, Z_a]) = [\alpha_1^*, \ldots, \alpha_n^*] \rightarrow f(k \cdot [X_a, Y_a, Z_a]) = k \cdot [\alpha_1^*, \ldots, \alpha_n^*]$, for $k \geq 0$. The relevance of this property is highlighted in Fig. 4, in which we compare the upsampling produced by the CFNN with the one by a vanilla MLP, on the same input tristimulus values, derived by a spectrum at 3 different intensities.

To create our training set, we make use of the illumination spectra from the Lamp SPD Database [†] (LSPDD), which includes measured spectra of different kind of lamps, including compact fluorescent, halogen, high pressure sodium, incandescent, LED and metal halide, as well as standard illuminants. Out of the 311 available spectra, we select 144 by removing near-duplicate ones, and include 16 daylight spectra, for a total of 160 illuminants. Overall, the dataset is balanced in terms of different illuminant types. For each illuminant, we also compute the spectra reflected off the 1269

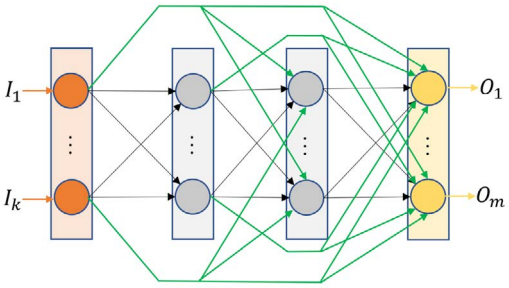

Figure 3: *Schematic representation of a CFNN with k inputs, m outputs and two hidden layers (highlighted in grey). In black the connections in common with a feed-forward network with fully connected layers, in green the additional connections introduced in the CFNN architecture.*

Figure 4: *Upsampling produced by the CFNN (on the left) and a vanilla MLP (on the right) on the same inputs, given by the XYZ values of a spectrum at 3 different levels of intensity. While both architectures produce plausible results, the CFNN output leads to spectra with very similar shapes. The output of the vanilla MLP is less regular, as noticeable on the peaks at around 630nm. Both networks share the same number of layers and neurons, and have been trained in the same way.*

matt Munsell color chips; the resulting 203,200 spectra are then converted to their tristimulus representation. Finally, the dataset is augmented by scaling spectra and corresponding weights by a set of predefined constants. To estimate the set of weights α_k^*, we rely on a modified version of the GA described in Sec. 3.2 (without initialization). While the input to the genetic algorithm are still tristimulus values, since in this case the ground truth spectra are known, we augment the fitness function with the cosine similarity between the ground truth and the reconstructed spectrum, in order to estimate weights for our basis that preserve both the ground truth shape and the corresponding tristimulus value as much as possible.

The architecture of our network consists of 3 hidden layers H_i, with decreasing number of nodes as their depth increases ($|H_1| = 13$, $|H_2| = 11$, $|H_3| = 8$) and hyperbolic tangent activation function. In our experiments, additional hidden layers did not lead to better results, while using just two hidden layers affects the performance, particularly in case of saturated input colors. The number of neurons per layer reported in the above is the smallest possible without causing a drop in the performance. As for the final layer, with $n = 6$ nodes directly providing in output the activation weights for the spectra in our basis, we use the ReLU function. The network is trained using Bayesian regularization backpropagation [Mac92],

† https://lspdd.org/

which pushes unnecessary weights towards zero, thus "pruning" the network. Along with the balanced dataset, the regularization helps avoiding overfitting and ensuring the network is able to generalize well. The loss given by the mean squared error between predicted and ground truth weights. At run-time, the CFNN can upsample one color in 5.58×10^{-7}s (unoptimized implementation on 1 thread of CPU, on the same hardware as in Sec. 3.2).

4. Evaluation

We now evaluate our choice of basis and our approach against measured ground truth spectra (Sec. 4.1), and show applications of the method for spectral upsampling of existing HDR environments for spectral lighting reproduction (Sec. 4.2 and Sec. 4.3). Sec. 4.4 demonstrates the quality of the metamers produced by our method, by comparing the appearance of a color chart under the metameric illumination with its appearance under ground truth illumination. In Sec. 4.6 we compare our direct spectral upsampling approach against the approach of [LYL*16] which requires additional measurements of reference colorcharts under target lighting. We additionally compare to existing methods for RGB to spectral upsampling which focus on reflectance [MY19, JH19, TWF21] and show that, as discussed in their work, the spectrum smoothness assumption does not hold for many illuminants. While most of the previous works are limited to sRGB upsampling, our method can address colors well beyond the sRGB gamut and it is suitable for wide-gamut color spaces. Since our method is not tied to a specific basis, the actual gamut effectively covered depends on the selected one. To demonstrate the method generalizes to other basis, we propose a theoretical Gaussian basis and that achieve higher accuracy than LEDs. Therefore, we show the suitability of our method for spectral upsampling and representation of illumination for spectral rendering applications (Sec. 4.5).

4.1. Recovered spectra evaluation

We evaluate our method by comparing the results to measured spectra and RGB color of both outdoor illuminants (HDR environment map regions) and indoor illuminants (Philips Hue LEDs).

4.1.1. Outdoors illuminant

In the case of outdoor illumination, our ground-truth comes from the BGU iCVL Hyperspectral Image Dataset [ABS16], containing HDR and spectral captures of outdoor scenes.

For this evaluation we use the RGB color as input to our method and the spectral measurements as ground-truth. For each environment, we determine our target reference color by averaging the color of the dominant illuminant – usually a patch of sky or the sun. For the BGU iCVL Hyperspectral Image Dataset, we average the spectra of the pixels used to determine our target reference color and use this average spectra as the ground truth SPD.

We show two examples of the results of our optimization on the spectral database in Fig. 5. The SPD reconstructed by our optimization closely approximates the shape of the spectral data, as well as the reference RGB color. By using the estimated SPDs to illuminate a color chart, we obtain an average ΔE_{94} difference of 1.3714 across the 6 evaluated RGB colors of outdoor illuminants.

4.1.2. Indoors illuminant

Further, we evaluate our methods on indoor lighting conditions as they exhibit very different spectra compared to natural illumination. To do so, we capture HDR images and measure spectra of different colors of Philips Hue LED lamps in a dark room. Fig. 6 shows results generated for different colors of the LED lamp. Similarly to outdoor illuminants, our method matches well the ground-truth.

4.2. Multispectral lighting reproduction

We show benefit of our proposed spectral upsampling of RGB illumination for lighting reproduction in Fig. 7. We show several objects recorded under both indoor and outdoor environmental illumination where we acquired the corresponding RGB light probe with HDR imaging. We drive our multispectral LED sphere directly with the recorded RGB illumination, as well as our proposed spectral upsampling to drive all 6 LED types on the LED sphere for spectral lighting reproduction. For the spectral lighting case, the optimized weights of our LED basis are directly used to drive the intensity of each LED type on the LED sphere. As can be seen, the lighting reproduction achieved with our spectral upsampling step is a better match to the input photograph of the objects compared to RGB lighting. This is consistent with the findings of LeGendre et al. [LYL*16] (despite our method *not* requiring reference color chart measurements), providing a qualitative validation of our spectral upsampling method. Fig. 1 shows another example of our method used for driving spectral lighting reproduction.

4.3. Spectral upsampling of environment maps

We also use our method for spectral upsampling of pre-recorded RGB environment maps. Fig. 8 shows results generated for Grace Cathedral environment map. Here, the RGB pixels of the original environment map were processed using our method to obtain weights of the 6 LED types in our basis which are shown as the 6 weight maps color coded with the color produced by the corresponding LED type. Fig. 8 also shows the reconstructed RGB colors produced by the weighted combination of the 6 LEDs which is a very close match to the input RGB colors in the environment map. The maximum error in the reconstructed environment illuminations is in the Grace Cathedral example with $\Delta E_{94} = 0.9525$. We provide additional examples of such spectral upsampling of environment maps in the Supplemental material.

4.4. Color checker validation

In Figs. 9, 10, 12 & 13, we compare the result of our method with the ground truth spectra using color chart renderings. We illuminate each color chart patch with the ground truth and the recovered spectra, and visualize the two colors in the same image, where for each patch the inner circle corresponds to the color produced with our or competing methods and the outer frame represents the ground truth color. The RGB values of each patch are generated by convolving the illumination spectrum, the known X-Rite color chart patches reflectances [‡] and the CIE 1931 2-degree CMFs, which is followed by standard XYZ to RGB conversion. For error computation we use the CIE Lab space, to which we convert XYZ values using standard

‡ https://www.babelcolor.com/colorchecker.htm

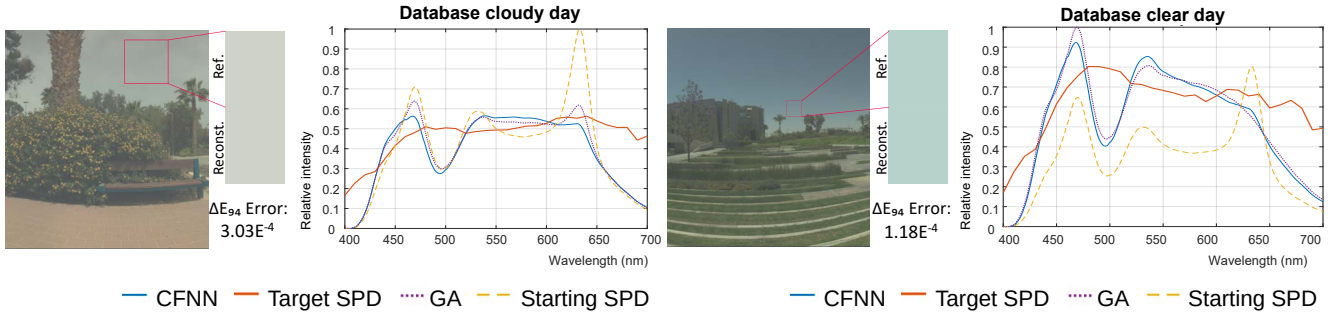

Figure 5: *Some results of our optimization (in dotted yellow is our initialization) for outdoor environment illumination from the iCVL Hyperspectral Database Portal. The photographs are generated from the provided measured spectral data using CIE 1931 2-degree CMFs, as only spectral data are available. In all cases we tested we find a close metamer and spectral match for both cloudy and clear day.*

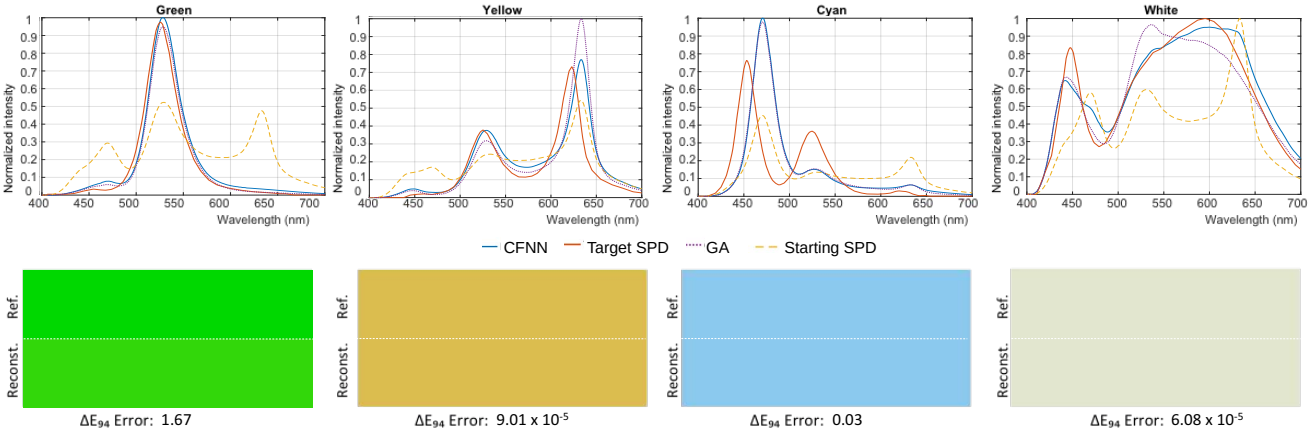

Figure 6: *We evaluate our approach on indoor illuminants (Philips Hue) we measured. For all results, our method very closely match the target color (Ref.) and its spectrum. We show in dotted yellow the result of our initialization.*

XYZ to CIE Lab conversion. We observe that our predicted spectrum is an excellent metamer for the target spectrum in almost all of the cases we tested. This is particularly interesting for the case of outdoor illumination, with a flatter spectrum compared to indoor illumination. While our basis fits non-smooth indoor illumination spectrum with higher accuracy, our optimized spectrum for outdoor illumination is still an excellent metamer.

4.5. Basis evaluation

While we chose our basis to enable environment lighting reproduction in the LED-sphere that we have access to, other spectral bases can also be used with our method. We evaluate our approach on other 6-illuminants bases as previous works [LYL*16, GGD*20] have shown it to lead to good spectral and colorimetric accuracy, while keeping the basis compact with additional LEDs leading to marginal improvements. We show results of our method using the LED basis employed by LeGendre et al. [LYL*16] and discuss a theoretical basis based on narrow and broad Gaussians which can be used for RGB-to-spectral illumination upsampling.

4.5.1. RGBCAW LED Basis

An alternate LED basis installed on USC ICT's Lightstage X includes RGBW LEDs similar to our own basis, but contains only one broad band white instead of our three types. Instead, this basis includes two additional narrow band illuminants covering the amber and cyan spectrum (see Supplemental material).

We show in Fig. 9 a comparison of rendered patches of a color chart under various illumination spectra recovered using our basis (RGBW+) against the RGBCAW basis, as described in Sec. 4.4. We find that our basis represents indoor illuminants slightly better while the RGBCAW basis works slightly better for outdoor illuminants. When comparing the average ΔE_{94} error over all colorchecker patches across both outdoor and indoor evaluated illuminant colors, both bases are relatively close with $\Delta E_{94} = 1.8658$ for ours and $\Delta E_{94} = 2.7350$ for RGBCAW.

4.5.2. Gaussian basis

While our primary basis selection was based on practical reasons such as using commonly available LEDs for lighting reproduction, we also perform analysis on synthetically computed spectral bases

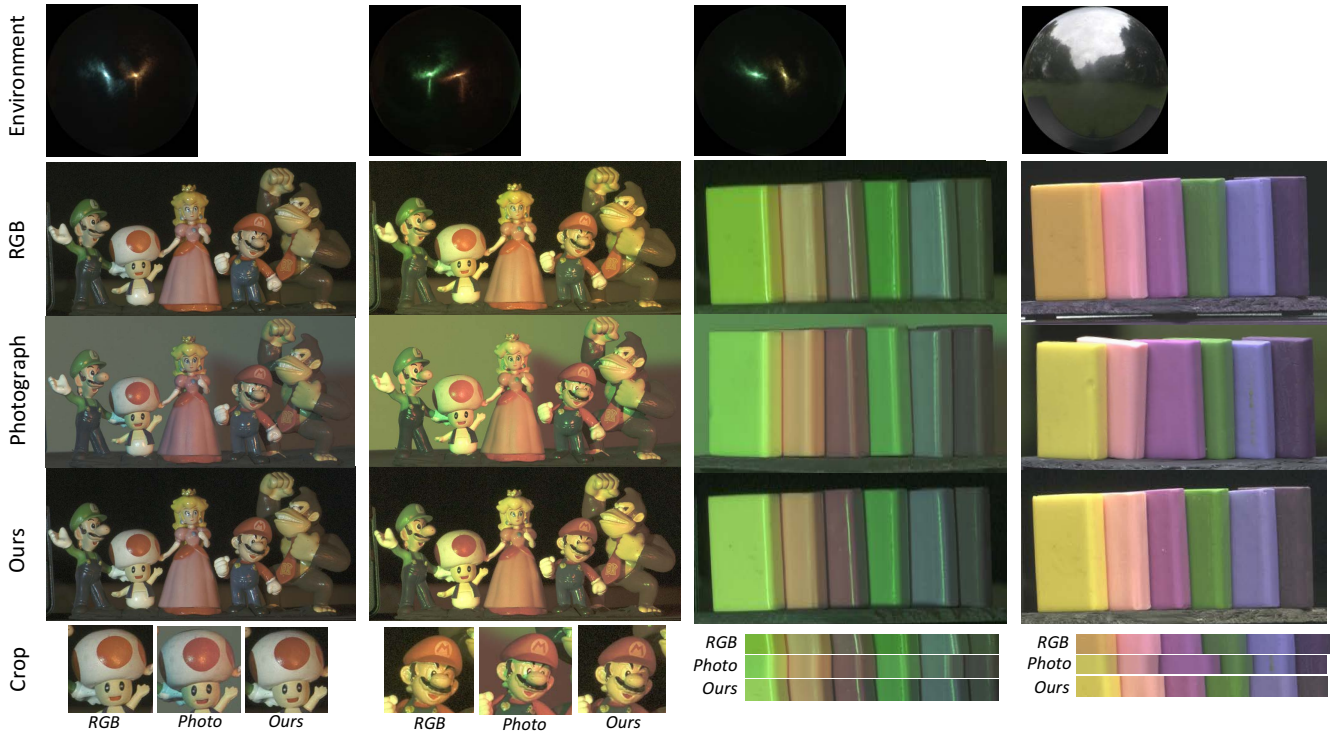

Figure 7: *Comparison of photographs of objects under environment illumination, under reproduced RGB illumination using RGB LEDs, and under reproduced spectral illumination using our approach. Qualitatively, our method allows more accurate reproduction of the lighting.*

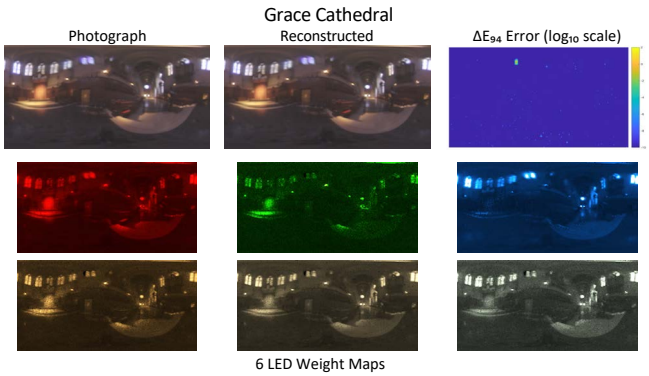

Figure 8: *Spectral upsampling of an RGB environment map. Top row shows original and reconstructed RGB environment map as well as ΔE_{94} error between the two images. Middle and bottom rows show weight maps for each basis spectrum converted to RGB using CIE 1931 CMFs.*

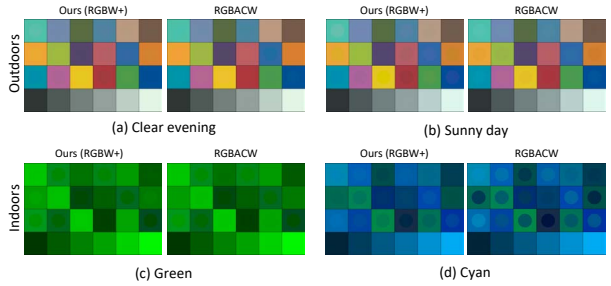

Figure 9: *Color chart comparison –as described in Sec. 4.4– of our RGBW+ basis vs. RGBCAW spectral basis for outdoor and indoor illumination spectra. Both bases produce very comparable overall results, with the RGBW+ basis producing slightly better results for indoor illumination (c, d).*

consisting of a set of narrow and broad Gaussian functions. We chose Gaussians for our analysis as they are compact in representation (requiring only 2 values), have shapes that are similar to LED responses, and have been previously employed in realistic rendering pipelines (e.g. the Gaussian Spectrum node for texture reflectance and textured emission in Octane Render [§]). To find the best Gaussian bases, we create different sets of narrow- and broad-band spectra using Gaussian functions with specified width (standard deviation) and peak locations (mean). For the narrow band set of Gaussians we place each peak at 25nm distance from each other in the visible wavelength range (400-700nm) and use standard deviation of 15nm. For the broad band set we increase the standard

§ https://docs.otoy.com/Portal/Home.htm

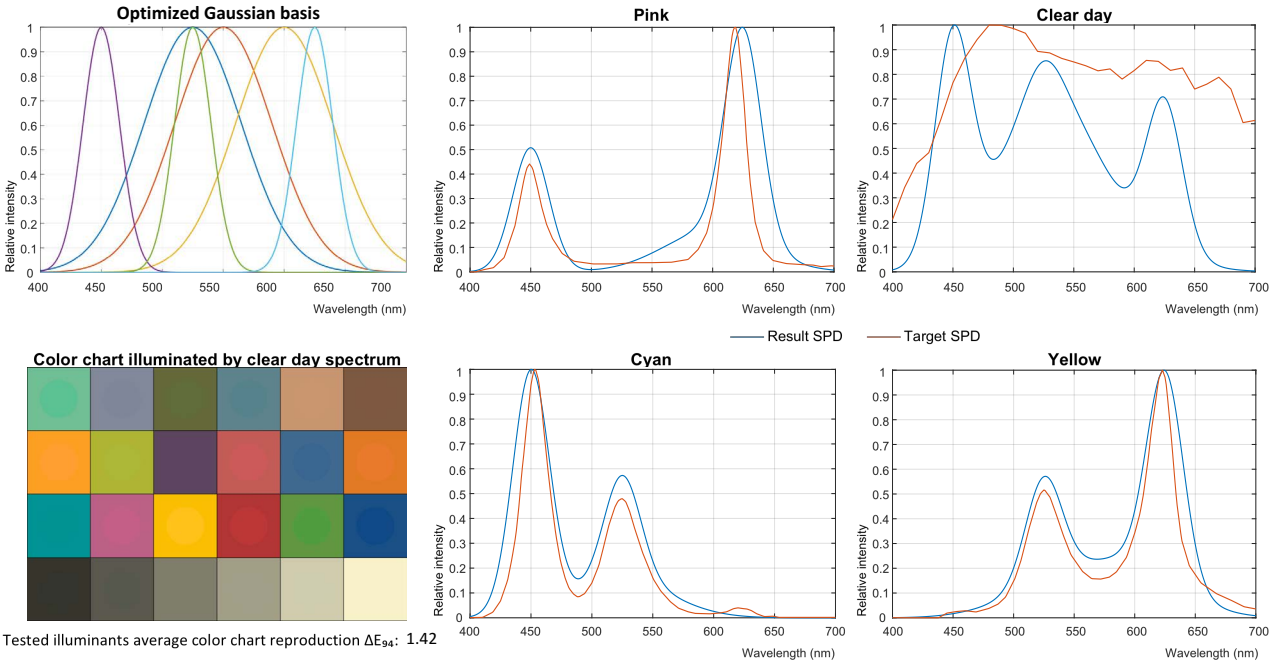

Figure 10: *SPD optimization results for the Gaussian spectra with basis consisting of 3 broad and 3 narrow bands and color chart evaluation –as described in Sec. 4.4–. The individual ΔE_{94} errors for Pink, Clear day, Cyan and Yellow examples are 1.81, 1.41, 1.55 and 1.58 respectively. The selected basis is the optimal basis producing the least LAB total error for the 12 tested illuminants. While similar to our LED basis, the Gaussian basis allows to better reconstruct illuminants than the RGBW+ and RGBACW LED bases.*

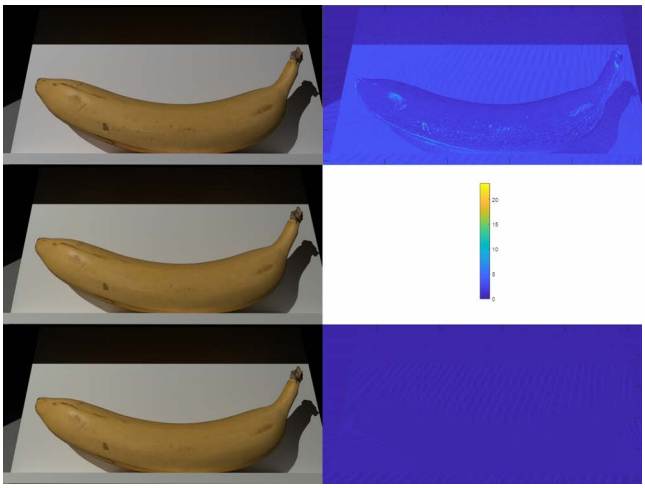

Figure 11: *Comparison of full ground truth spectral rendering under D65 illumination (middle row), with a RGB rendering using for the illuminant the RGB values corresponding to D65 (top row), and rendering with spectral upsampling of RGB using our optimized Gaussian basis (bottom row). The result of our spectral upsampling is indistinguishable from the reference rendering, while color differences in the RGB rendering are clearly visible.*

deviation to 40nm. We ran our optimization on all possible combinations of this initial selection of Gaussians (see supplemental materials), specifying the number of broad and narrow bands to include. Finally, for each distribution of broad and narrow bands, we choose the set of Gaussians which produces the smallest total ΔE_{94} Lab error between the target and the reconstructed color across all evaluated indoor and outdoor illuminants. The error can be slightly improved by including more spectra, but with diminishing returns, particularly towards the UV and IR edges of the visible spectrum due to limitations of the human visual system.

We show in Fig. 10 the results of this search with 3 narrow band spectra and 3 broad band spectra which provides a slight improvement in matching of the target illumination spectrum compared to our LED basis. Interestingly, we can see that the set of optimized Gaussians bear a strong similarity to our employed RGBW+ LED basis, with the three narrow bands corresponding to RGB color primaries and the three broadbands being slightly shifted between warmer and cooler spectra. The results discussed in the remainder of this section are obtained using the GA described in Sec. 3.2.

Given the slightly higher accuracy of the optimized Gaussian basis compared to the LED bases, it can be a good choice for spectral upsampling and representation of illumination for spectral rendering applications. Fig. 11 shows rendering comparisons of a scene consisting of a banana on a ceramic bowl that is rendered with a D65 illuminant with full spectral rendering (sampling at every 2nm intervals, middle row) using Mitsuba2. The corresponding rendering with RGB illumination with RGB values set to (1, 1, 1) results in noticeable difference (top row) compared to the reference spec-

tral rendering, particularly on the white ceramic and color of the banana. Finally, our RGB-to-spectral upsampling using our optimized Gaussian basis results in a rendering that is nearly indistinguishable (bottom row) from the full spectral rendering. In the supplemental, we report a rendering comparison for a narrowband illuminant.

Taking a cue from the RGBCAW LED basis, we additionally experimented with Gaussian bases containing 5 narrowband spectra and 1 broadband spectra. However, the best average ΔE_{94} (1.8545) was slightly worse than that with 3 narrowband and 3 broadband spectra ($\Delta E_{94} = 1.3970$). In the supplemental we report a table with the average ΔE_{94} for each basis on color checker illumination, as described in Sec. 4.4. Both set of Gaussian bases result in $\Delta E_{94} < 2$, typically considered as a good match and significantly better than the acceptability threshold in graphics art and display technology. We found the analysis with Gaussian bases to be consistent with the performance of the RGBW+ vs RGBCAW LED bases.

4.6. Comparisons

4.6.1. Colorchart-based optimization

We compare our spectral upsampling technique to reference colorchart-based optimization similar to that employed by LeGendre et al. [LYL*16] for spectral lighting reproduction. Instead of solving for an entire environment map using five oriented colorcharts as done in [LYL*16], we perform a simpler comparison using a single reference colorchart illuminated with mostly frontal illumination emitted from a Philips Hue LED bulb. The colorchart-based optimization then searches for weights of the six colorchart responses due to the RGBW+ LEDs in the multispectral lightstage whose linear combination then minimizes the ΔE_{94} color differences over the set of 24 colors measured on the reference colorchart under a target illumination. The six optimized LED weights using the reference colorchart construct a predicted spectrum for the illumination through their linear combination. We repeat this for four different types of hues emitted by the LED bulb (see Fig. 12). We measure the target ground truth spectrum for each illumination condition using a spectrometer. Finally, we also predict the spectra for each of the illumination conditions using our proposed method directly from the RGB values of the illumination recorded on a mirror ball. As can be seen in Fig. 12, our spectral upsampling method predicts spectra of very comparable (or in some cases even better) quality than [LYL*16], *without* requiring measurements of a reference colorchart. Thus, our method removes the requirement of specialized measurement of oriented colorcharts for environmental illumination, thereby enabling direct spectral upsampling of legacy RGB light probes for spectral lighting reproduction.

4.6.2. Reflectance spectrum upsampling

We compare to recent RGB-to-spectral upsampling techniques of Mallett & Yuksel [MY19] and Jakob & Hanika [JH19] which are designed for smooth reflectance spectrum. In Fig. 13 we show comparisons to our method on illuminants (White and Green). For each spectrum, we show the target and the resulting spectra recovered with each method, as well as a color chart comparison –as described in Sec. 4.4. This comparison illustrates the limitations of the smoothness assumption when recovering illuminants, as described in previous work [JH19, MY19]. Additionally, we show that, while not its primary purpose, our method is also capable of recovering reasonable metamer spectra for reflectance (included in Supplemental). This confirms that our method can upsample entire RGB environment maps, which typically not only consist of illuminants, but also background pixels which represent reflectances convolved with illuminants. Fig. 13 also includes comparison to an unconstrained variant of the recently proposed method of Tódová et al. [TWF21]. Note that their constrained method is designed to be used with user provided bases, but is limited to the sRGB gamut which does not apply for illumination spectrum. The results of the unconstrained variant of [TWF21] are similar to that of [JH19].

4.7. Limitations

Our method shares some inherent limitations with previous work: in the absence of additional information, other than an RGB color, to guide the basis optimization, the solution can at best converge to a metamer of the target of illumination. In some cases we tested, we found the LED basis we employed did not converge to a spectrum that provides a perfect RGB color match (see Fig. 14), although this is alleviated to a great extent with our Gaussian basis. Due to the shapes of the chosen bases (LEDs or Gaussians), the method also does not perfectly match target flat spectra typical of natural outdoor illumination, particularly near the two extremes of the visible spectrum. However, our method still produces very good metamers for such outdoor illumination spectra.

5. Conclusion

We introduced two practical methods for high fidelity spectral upsampling of recorded RGB illumination using a chosen set of illumination bases and optimizing their convex combination to best match an input RGB color. Our method does not require any additional information such as reference color chart measurements, making it suitable for directly applying it for upsampling of legacy RGB lighting environments for improved spectral rendering as well as lighting reproduction. We demonstrate good qualitative matches to ground truth spectra for a range of measured outdoor and indoor illumination and also demonstrate the benefit of the approach over existing spectral upsampling techniques designed for smooth reflectance spectra.

Acknowledgments

We thank Dar'ya Guarnera for the assets used in the spectral renderings. This work was partly supported by following: Spectraskin project N-288670, funded by the Research Council of Norway, a Rabin Ezra scholarship, and EPSRC Fellowship EP/N006259/1.

References

[ABS16] ARAD B., BEN-SHAHAR O.: Sparse recovery of hyperspectral signal from natural rgb images. In *European Conference on Computer Vision* (2016), Springer, pp. 19–34. 2, 6

[AG18] AKBARINIA A., GEGENFURTNER K. R.: Color metamerism and the structure of illuminant space. *J. Opt. Soc. Am. A 35*, 4 (Apr 2018), B231–B238. 2

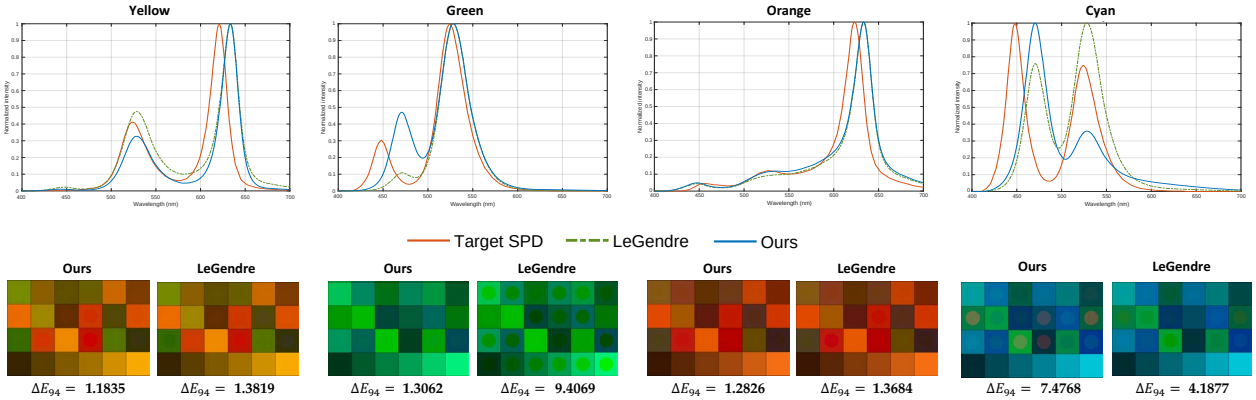

Figure 12: *Spectra of various illuminants predicted using reference colorchart-based optimization [LYL*16], and our proposed spectral upsampling method compared against target ground truth spectra (measured using a spectrometer). Both methods result in comparable high quality estimation of illumination spectra, with our method having the advantage of not requiring any reference colorchart measurement.*

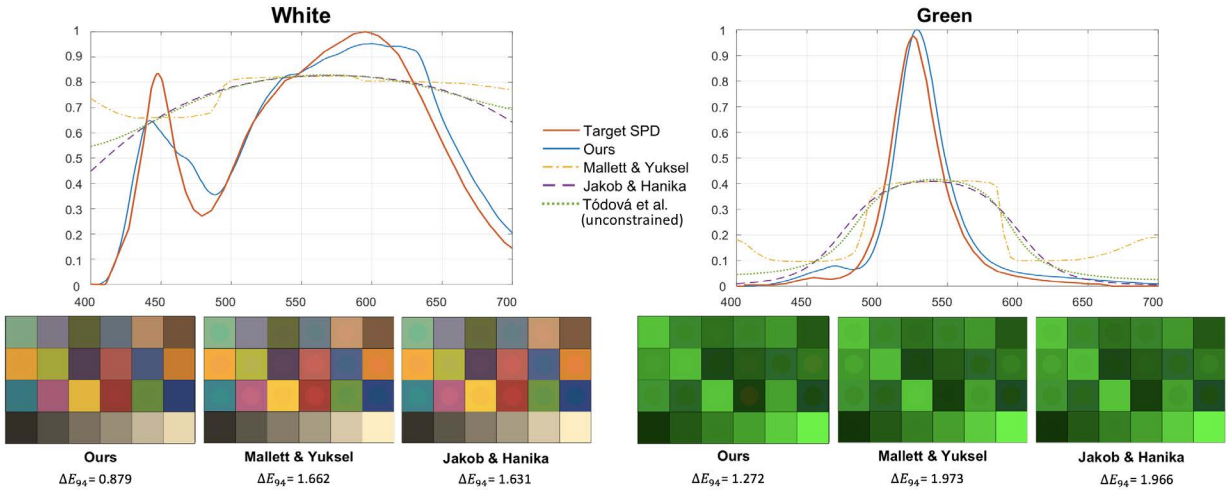

Figure 13: *We compare our method to Mallett & Yuksel [MY19] and Jakob & Hanika [JH19] for spectral upsampling of illuminants (White and Green). More examples for an outdoor illuminant (Clear evening) and a reflectance (Tiles) are included in the Supplemental. For each spectrum, we show the target and the resulting spectra recovered with each method, as well as color chart evaluations –as described in Sec. 4.4. We show that, as described in their papers, the spectrum smoothness assumption they use for reflectance spectra does not hold for illuminants. We also compare to unconstrained variant of the recent method of [TWF21] which is very similar to [JH19].*

[BCS17] BIANCO S., CUSANO C., SCHETTINI R.: Single and multiple illuminant estimation using convolutional neural networks. *IEEE Transactions on Image Processing 26*, 9 (2017), 4347–4362. 3

[Bia10] BIANCO S.: Reflectance spectra recovery from tristimulus values by adaptive estimation with metameric shape correction. *J. Opt. Soc. Am. A 27*, 8 (Aug 2010), 1868–1877. 3

[CIE86] CIE: Publication 15.2-1986 colorimetry, 2nd edition. *Tech report* (1986). 2

[CIE95] CIE: Publication 116-1995 industrial colour-difference evaluation. *Tech report* (1995). 4

[Dav51] DAVID F. N.: *Probability theory for statistical methods*. Cambridge: The University Press, 1951. 4

[Deb98] DEBEVEC P.: Rendering synthetic objects into real scenes: Bridging traditional and image-based graphics with global illumination and high dynamic range photography. In *Proceedings of the 25th Annual Conference on Computer Graphics and Interactive Techniques* (New York, NY, USA, 1998), SIGGRAPH '98, Association for Computing Machinery, p. 189–198. 2

[DGBB12] DEBEVEC P., GRAHAM P., BUSCH J., BOLAS M.: A single-shot light probe. In *ACM SIGGRAPH 2012 Talks* (New York, NY, USA, 2012), SIGGRAPH '12, Association for Computing Machinery. 2

[DHT*00] DEBEVEC P., HAWKINS T., TCHOU C., DUIKER H.-P., SAROKIN W., SAGAR M.: Acquiring the reflectance field of a human face. In *Proceedings of the 27th Annual Conference on Computer Graphics and Interactive Techniques* (USA, 2000), SIGGRAPH '00, ACM Press/Addison-Wesley Publishing Co., p. 145–156. 2

[DSKM09] DEEP K., SINGH K. P., KANSAL M., MOHAN C.: A real coded genetic algorithm for solving integer and mixed integer optimization problems. *Applied Mathematics and Computation 212*, 2 (2009), 505–518. 4

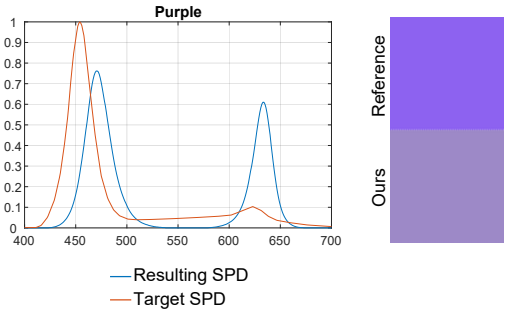

Figure 14: *For some tested colors, such as this shade of purple, our method does not provide a perfect RGB color match due to physical limitations of the employed LED basis.*

[Ebn07] EBNER M.: *Color Constancy*. The Wiley-IS&T Series in Imaging Science and Technology. Wiley, 2007. 3

[FF12] FENG G., FOSTER D. H.: Predicting frequency of metamerism in natural scenes by entropy of colors. *J. Opt. Soc. Am. A 29*, 2 (Feb 2012), A200–A208. 2

[FRJ01] FAIRCHILD M. D., ROSEN M. R., JOHNSON G. M.: Spectral and metameric color imaging. *Technical Report, RIT-Munsell Color Science Laboratory* (2001). 2

[FSD20] FUBARA B. J., SEDKY M., DYKE D.: Rgb to spectral reconstruction via learned basis functions and weights. In *2020 IEEE/CVF Conference on Computer Vision and Pattern Recognition Workshops (CVPRW)* (2020), pp. 1984–1993. 3

[GBS19] GUARNERA G. C., BIANCO S., SCHETTINI R.: Turning a digital camera into an absolute 2d tele-colorimeter. *Computer Graphics Forum 38*, 1 (2019), 73–86. 3, 4

[GGD*20] GITLINA Y., GUARNERA G. C., DHILLON D. S., HANSEN J., LATTAS A., PAI D., GHOSH A.: Practical measurement and reconstruction of spectral skin reflectance. *Computer Graphics Forum 39*, 4 (2020), 75–89. 7

[Gra53] GRASSMANN H.: Zur theorie der farbenmischung. *Annalen der Physik 165*, 5 (1853), 69–84. 3

[GRB*08] GEHLER P. V., ROTHER C., BLAKE A., MINKA T., SHARP T.: Bayesian color constancy revisited. In *2008 IEEE Conference on Computer Vision and Pattern Recognition* (2008), pp. 1–8. 3

[Har01] HARDEBERG J. Y.: *Acquisition and reproduction of color images: colorimetric and multispectral approaches*. Universal Publishers, 2001. 2, 3

[HFG*20] HEMRIT G., FINLAYSON G. D., GIJSENIJ A., GEHLER P., BIANCO S., DREW M. S., FUNT B., SHI L.: Providing a single ground-truth for illuminant estimation for the colorchecker dataset. *IEEE Transactions on Pattern Analysis and Machine Intelligence 42*, 5 (2020), 1286–1287. 3

[JH19] JAKOB W., HANIKA J.: A low-dimensional function space for efficient spectral upsampling. *Computer Graphics Forum (Proceedings of Eurographics) 38*, 2 (Mar. 2019). 2, 3, 6, 10, 11

[JWH*19] JUNG A., WILKIE A., HANIKA J., JAKOB W., DACHSBACHER C.: Wide gamut spectral upsampling with fluorescence. *Computer Graphics Forum 38*, 4 (2019), 87–96. 3

[KK08] KIM M. H., KAUTZ J.: Characterization for high dynamic range imaging. *Computer Graphics Forum 27*, 2 (2008), 691–697. 3

[LYD17] LEGENDRE C., YU X., DEBEVEC P.: Optimal led selection for multispectral lighting reproduction. *Electronic Imaging 2017*, 8 (2017), 25–32. 2

[LYL*16] LEGENDRE C., YU X., LIU D., BUSCH J., JONES A., PATTANAIK S., DEBEVEC P.: Practical multispectral lighting reproduction. *ACM Trans. Graph. 35*, 4 (July 2016). 2, 3, 4, 6, 7, 10, 11

[Mac92] MACKAY D. J. C.: Bayesian Interpolation. *Neural Computation 4*, 3 (05 1992), 415–447. 5

[MSHD15] MENG J., SIMON F., HANIKA J., DACHSBACHER C.: Physically meaningful rendering using tristimulus colours. *Computer Graphics Forum 34*, 4 (2015), 31–40. 3

[MY19] MALLETT I., YUKSEL C.: Spectral Primary Decomposition for Rendering with sRGB Reflectance. In *Eurographics Symposium on Rendering - DL-only and Industry Track* (2019), Boubekeur T., Sen P., (Eds.), The Eurographics Association. 2, 3, 6, 10, 11

[NDVZJ19] NIMIER-DAVID M., VICINI D., ZELTNER T., JAKOB W.: Mitsuba 2: A retargetable forward and inverse renderer. *ACM Trans. Graph. 38*, 6 (Nov. 2019). 2

[PJH16] PHARR M., JAKOB W., HUMPHREYS G.: *Physically Based Rendering: From Theory to Implementation*. Morgan Kaufmann, 2016. 2

[PLGN07] PARK J., LEE M., GROSSBERG M. D., NAYAR S. K.: Multispectral imaging using multiplexed illumination. In *2007 IEEE 11th International Conference on Computer Vision* (2007), pp. 1–8. 2

[PMHD19] PETERS C., MERZBACH S., HANIKA J., DACHSBACHER C.: Using moments to represent bounded signals for spectral rendering. *ACM Trans. Graph. 38*, 4 (July 2019). 2, 3

[RHA11] RATNASINGAM S., HERNÁNDEZ-ANDRÉS J.: Illuminant spectrum estimation at a pixel. *J. Opt. Soc. Am. A 28*, 4 (Apr 2011), 696–703. 3

[SYH*14] SHI J., YU H., HUANG X., CHEN Z., TAI Y.: Illuminant spectrum estimation using a digital color camera and a color chart . In *Optoelectronic Imaging and Multimedia Technology III* (2014), Dai Q., Shimura T., (Eds.), vol. 9273, International Society for Optics and Photonics, SPIE, pp. 1 – 9. 3

[TF07] TOMINAGA S., FUKUDA T.: Omnidirectional scene illuminant estimation using a multispectral imaging system. In *Color Imaging XII: Processing, Hardcopy, and Applications* (2007), Eschbach R., Marcu G. G., (Eds.), vol. 6493, International Society for Optics and Photonics, SPIE, pp. 352 – 359. 3

[Tom96] TOMINAGA S.: Multichannel vision system for estimating surface and illumination functions. *J. Opt. Soc. Am. A 13*, 11 (Nov 1996), 2163–2173. 3

[TT06] TOMINAGA S., TANAKA N.: Omnidirectional scene illuminant estimation using a mirrored ball. *Journal of Imaging Science and Technology 50*, 3 (2006), 217–227. 3

[TWF21] TÓDOVÁ L., WILKIE A., FASCIONE L.: Moment-based Constrained Spectral Uplifting. In *Eurographics Symposium on Rendering - DL-only Track* (2021), The Eurographics Association. 3, 6, 10, 11

[UWH*03] UNGER J., WENGER A., HAWKINS T., GARDNER A., DEBEVEC P.: Capturing and Rendering With Incident Light Fields. In *Eurographics Workshop on Rendering* (2003), Dutre P., Suykens F., Christensen P. H., Cohen-Or D., (Eds.), The Eurographics Association. 2

[Wan87] WANDELL B. A.: The synthesis and analysis of color images. *IEEE Transactions on Pattern Analysis and Machine Intelligence PAMI-9*, 1 (1987), 2–13. 3

[WHD03] WENGER A., HAWKINS T., DEBEVEC P.: Optimizing Color Matching in a Lighting Reproduction System for Complex Subject and Illuminant Spectra. In *Eurographics Workshop on Rendering* (2003), Dutre P., Suykens F., Christensen P. H., Cohen-Or D., (Eds.), The Eurographics Association. 2

[WS82] WYSZECKI G., STILES W. S.: *Color Science: Concepts and Methods, Quantitative Data and Formulae*. Wiley, 1982. 2

[WSSY18] WARSITO B., SANTOSO R., SUPARTI, YASIN H.: Cascade forward neural network for time series prediction. *Journal of Physics: Conference Series 1025* (may 2018), 012097. 5